Supplement of

Substantial organic impurities at the surface of synthetic ammonium sulfate particles

Junteng WU et al.

Correspondence to: junteng.wu@univ-amu.fr and anne.monod@univ-amu.fr

SI1. Statistical studies using AS particles since 2000

Article number in total	Optical properties	Hygroscopicity	Phase transition	Chemical reaction
219	44	115	49	62

AS mark	Related article number
Sigma-Aldrich/Merck	43
Fisher Chemical/Fluka	21
Alfa Aesar	7
Beijing Chemical Reagent	2
Mallinckrodt Baker	2
EMD Millipore	2
Tianjin	1
Shanghai Chemical and Medical Corporation	1
Univar	1
wako pure chemical	1
Not mentioned	137
In total	219

SI2 Reagents

Reagents	Mark and purity	Lot
Ammonium sulfate crystal	ACROS Organics from Fisher Chemical, 99.5%	A0408697
Ammonium sulfate crystal	Merck, EMSURE	AM1034817 833
Ammonium sulfate crystal	Merck suprapur, 99.9999%	B1675709
Liquid water	Milli-Q water, 18.2 MΩ cm, TOC < 2ppb	Laboratory product
Liquid water	Fisher Chemical, LC-MS Grade	2047076
Liquid Ethanol	Fisher Chemical, 99.8%	1922061
Hydrochloric acid	Fisher Chemical, Trace metal grade	4118060
Acetonitrile	Fisher Chemical, Optima© LC/MS grade	1924623
Methanol	Fisher Chemical, Optima© LC/MS grade	1737574

SI3 Raw mass spectra of CN compounds (EXP P1 at AS concentrations of 0.5M)

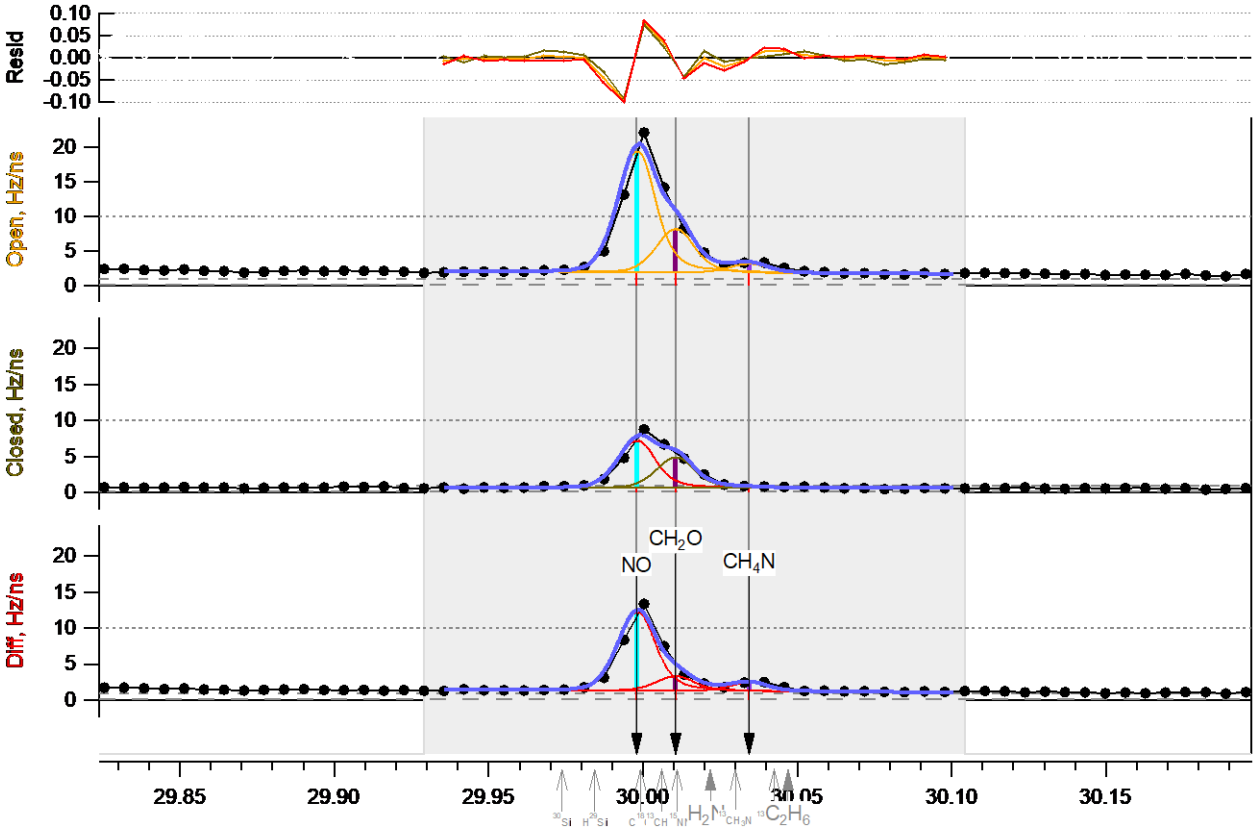

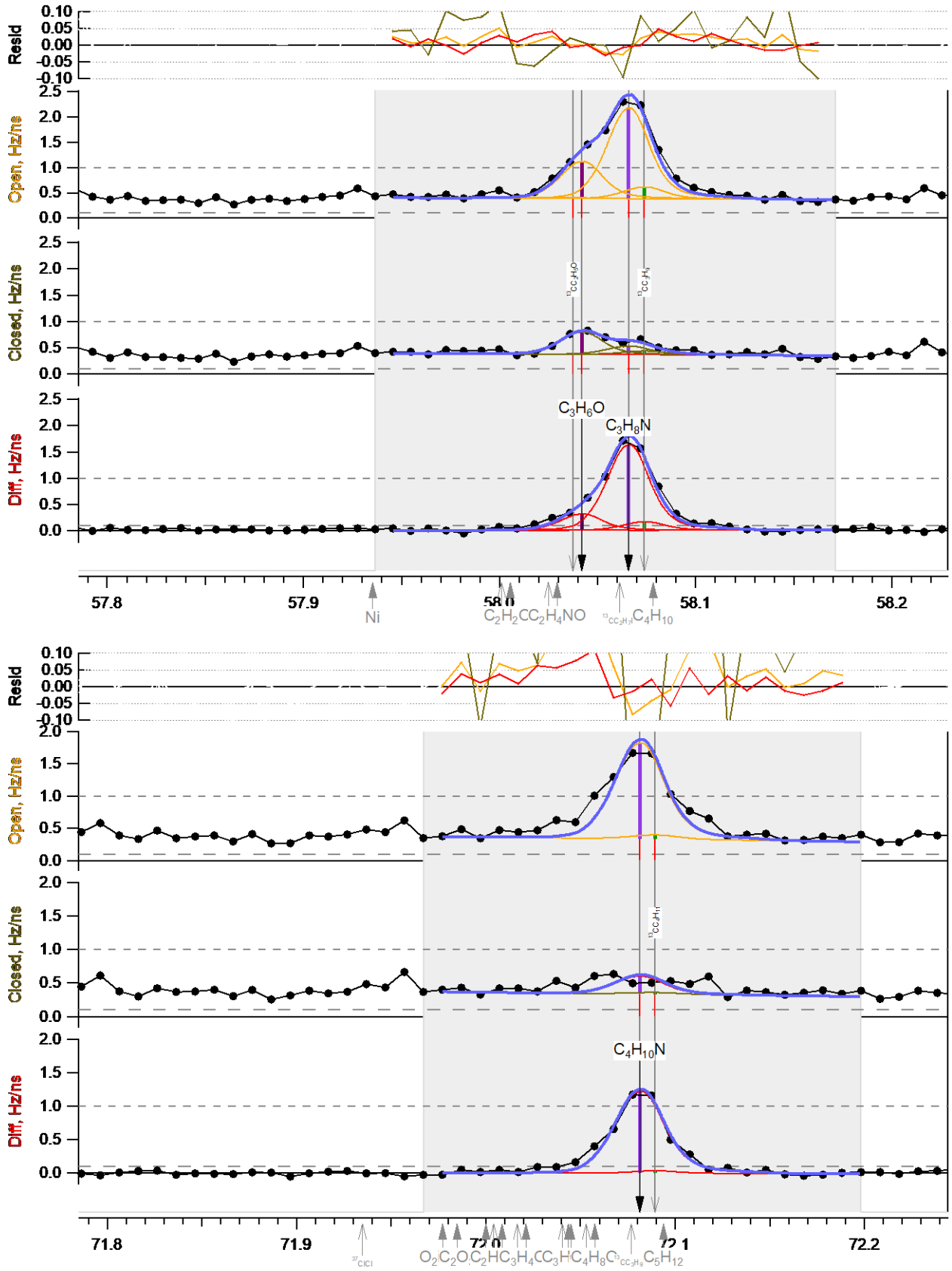
Resid
Open, Hz/ns
Closed, Hz/ns
Diff, Hz/ns
C3H6O
C3H8N
C4H10N
57.8
57.9
58.1
58.2
71.8
71.9
72.2
Ni
C2H2CC2H4NO
C4H10
C5H12

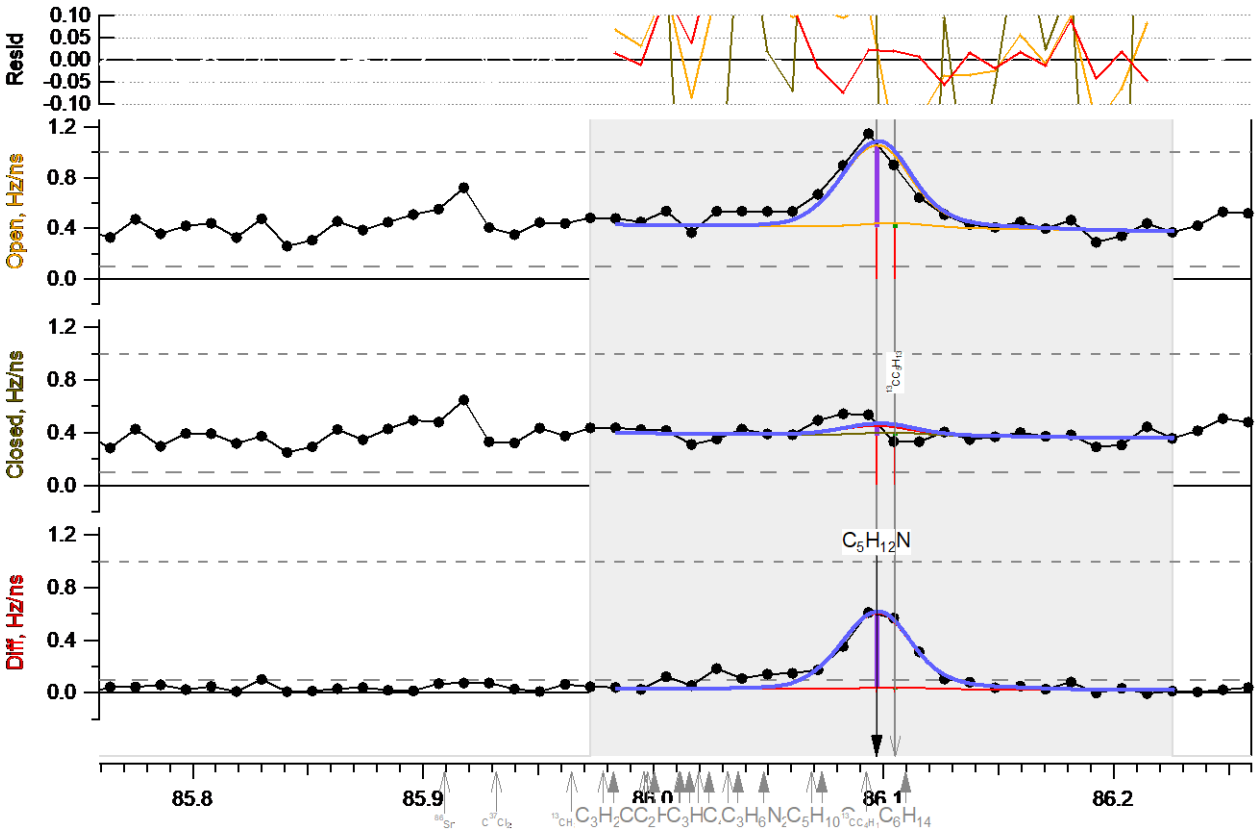

SI4 Influence of the AAC rotational speed on the chemical content

Developed by Tavakoli and Olfert (2013), AAC is a recent commercial aerosol classifier, it selects the size by centrifuge force. The aerodynamic diameter (d_a) of selected particles is related to the rotational speed of the concentric cylinder, the sheath flow rate and the sample flow rate. The rotational speed has been reported to influence the geometric standard deviation (σ_{geo}) of size distribution, i.e., the smaller size, the higher rotational speed and the larger σ_{geo} (Johnson et al., 2018). This behavior is also reported in this work and is shown in **Error! Reference source not found.**. To understand the influence of the rotational speed on the detection of organic traces, AS aerosols at d_a = 300 nm were selected in EXP P7 (Table 1) under three different rotational conditions: 190, 285 and 369 rad/s. In Figure SI4: , the ratios of mass concentrations Org/Sulfate and CN/Sulfate are shown as a function of the rotational speed of the concentric cylinder in green and blue dots, respectively. Their averages are 2.9±0.1% and 0.48±0.04%. No significant difference has been observed with varying the rotational speed of AAC.

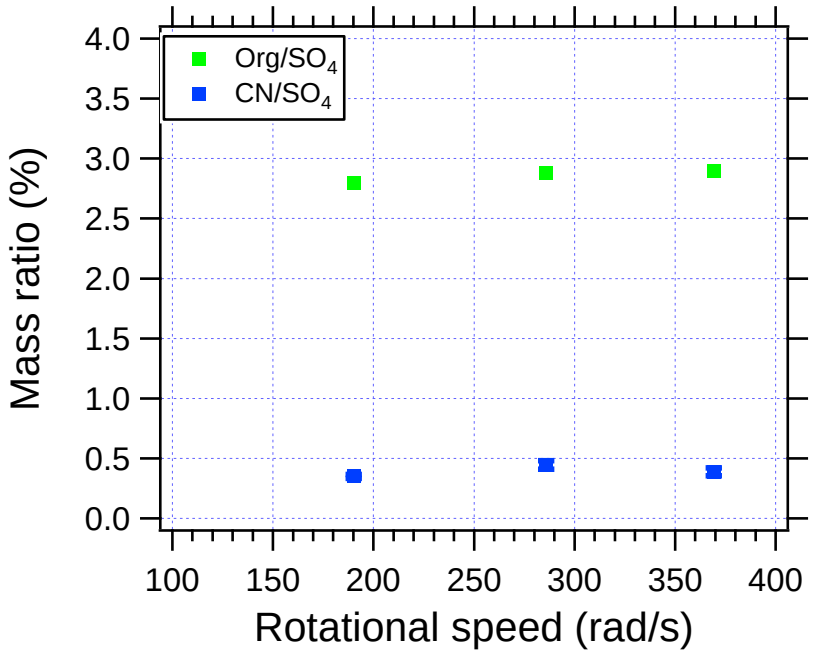

Figure SI4: Effect of the AAC rotational speed on the organic content in AS particles (at da = 300 nm) measured by the HR-ToF-AMS (in EXP P7).

SI5 Multi-charging corrections for the [Org]/[Sulfate] using the DMA for particle size selection

Under the hypothesis that organic compounds were coated homogenously on surface of AS aerosol particles, the density was defined as $\rho_{org,S}$. The correction was done by removing the effects of multi-charged modes, so the corrected [Org]/[Sulfate] were represented only by the first mode. In a first step, [Org]/[Sulfate] were calculated using equation SI5.1:

$$\frac{[Org]}{[Sulfate]}_{calc} = \frac{\sum_{1^{st}\ mode}(\pi d^2 N_d)\rho_{org,S}}{\sum_{1^{st}\ mode}\left(\frac{4}{3}\pi\frac{d^3}{2}\ N_d\right)\rho_{sulfate}} \qquad \text{Equation SI5.1}$$

Where N_d is the number concentration at diameter d, $\sum_{1^{st}\ mode}(\pi d^2 N_d)$ is the total surface of all particles in the first mode measured by SMPS. $\sum_{1^{st}\ mode}\left(\frac{4}{3}\pi\frac{d^3}{2}\ N_d\right)$ is the total volume of all particles in the first mode. $\rho_{sulfate}$ is the volume density of sulfate in AS aerosols, 96.06 g.cm^{-3}.

Experimentally, [Org]/[Sulfate] mass concentration ratios were measured by the HR-ToF-AMS which considered all the particle sizes (including multi-charged modes) as described by equation SI5.2:

$$\frac{[Org]}{[Sulfate]}_{exp} = \frac{\sum_{d=0}^{\infty}(\pi d^2 N_d)\rho_{org,S}}{\sum_{d=0}^{\infty}\left(\frac{4}{3}\pi\frac{d^3}{2}\ N_d\right)\rho_{sulfate}} \qquad \text{Equation SI5.2}$$

In the last step, combining Equation SI5.1 and Equation SI5.2, the corrected [Org]/[Sulfate] were obtained (equation SI5.3), they gather the total amounts of organics and sulfate on the first DMA mode:

$$\frac{[Org]}{[Sulfate]}_{corr} = \frac{\sum_{1^{st}\ mode} N_d d^2}{\sum_{1^{st}\ mode} N_d d^3} \times \frac{\sum_{d=0}^{\infty} N_d d^3}{\sum_{d=0}^{\infty} N_d d^2} \times \frac{[Org]}{[Sulfate]}_{exp} \qquad \text{Equation SI5.3}$$

Where all diameter information was recorded by the SMPS.

SI6 Majors ions detected in LC/ESI$^+$-MS of the aqueous solution of 1.5 M AS and their associated molecular formula and retention times.

m/z	Retention time	Proposed raw formula	Error (ppm)
96.0813	3.00	$C_6H_{10}N$	0
113.1078	**2.44**	**$C_6H_{13}N_2$**	0.9
209.1655	3.00	$C_{12}H_{21}N_2O$	0.5
223.1450	2.73	$C_{12}H_{19}N_2O_2$	1.3
225.1600	**3.02 ; 3.36**	**$C_{10}H_{21}N_2O_2$**	**1.3**
226.1918	**2.89 ; 3.11**	**$C_{12}H_{24}N_3O$**	**0.4**
227.1762	**3.51**	**$C_{12}H_{23}N_2O_2$**	**0.9**
241.1553	2.73 ; 3.01	$C_{12}H_{21}N_2O_3$	0.4
245.1862	3.21	$C_{12}H_{25}N_2O_3$	1.2
269.0962	2.86 ; 3.93	$C_{12}H_{17}N_2O_3S$	0.7
303.1012	2.76 ; 3.08	$C_{12}H_{19}N_2O_5S$	1
306.1487	2.89	$C_{12}H_{24}N_3O_4S$	0.3
307.1328	3.00	$C_{12}H_{23}N_2O_5S$	0
321.1117	2.73	$C_{12}H_{21}N_2O_6S$	0.9
340.2599	**3.97**	**$C_{18}H_{34}N_3O_3$**	**0.3**
343.0997	2.72	$C_{11}H_{23}N_2O_6S_2$	0.3
349.0528	2.55 ; 3.12	$C_{12}H_{17}N_2O_6S_2$	0
420.2164	3.49	$C_{18}H_{34}N_3O_6S$	1
456.1835	3.25	$C_{17}H_{34}N_3O_7S_2$	0.7
533.3006	3.88	$C_{24}H_{45}N_4O_7S$	0.6

In this table, the bold m/z were studied in more details using LC/ESI$^+$-MS-MS (shown in SI below).

SI7 LC/ESI$^+$-MS-MS of the most intense ions found in the acetonitrile liquid-liquid extracts of aqueous AS solution and their fragments (experiment C9).

Precursor ion m/z	Fragment ions m/z
113.108	96.082 ; 81.059 ; 79.056 ; 69.072
225.160	125.107 ; 113.108 ; 96.082 ; 85.030 ; 79.056 ; 69.072
226.192	114.092 ; 113.108 ; 96.082 ; 79.056 ; 72.082 ; 69.072
227.177	113.108 ; 96.082 ; 79.056 ; 69.072
340.260	228.160 ; 132.103 ; 114.092 ; 96.082 ; 69.072

Johnson, T. J., Irwin, M., Symonds, J. P. R., Olfert, J. S., and Boies, A. M.: Measuring aerosol size distributions with the aerodynamic aerosol classifier, Aerosol Sci. Technol., 52, 655–665, https://doi.org/10.1080/02786826.2018.1440063, 2018.

Tavakoli, F. and Olfert, J. S.: An Instrument for the Classification of Aerosols by Particle Relaxation Time: Theoretical Models of the Aerodynamic Aerosol Classifier, Aerosol Sci. Technol., 47, 916–926, https://doi.org/10.1080/02786826.2013.802761, 2013.